

# ELECTROACTIVE POLYMERS FOR THE DETECTION OF MORPHINE

**Esther Córdova-Mateo,<sup>1,2</sup> Jordi Poater,<sup>3</sup> Bruno Teixeira-Dias,<sup>1,4</sup> Oscar  
Bertran,<sup>2</sup> Francesc Estrany,<sup>4,5</sup> Luis J. del Valle,<sup>1</sup> Miquel Solà,<sup>3</sup> and  
Carlos Alemán<sup>1,4,\*</sup>**

<sup>1</sup> *Departament d'Enginyeria Química, ETSEIB, Universitat Politècnica de  
Catalunya, Av. Diagonal 647, 08028, Barcelona, Spain.*

<sup>2</sup> *Departament de Física Aplicada, EEI, Universitat Politècnica de Catalunya, Pça. Rei  
15, 08700 Igualada, Spain*

<sup>3</sup> *Institut de Química Computacional i Catàlisi (IQCC) and Departament de Química,  
Universitat de Girona, Campus de Montilivi, Girona E-17071, Spain*

<sup>4</sup> *Center for Research in Nano-Engineering, Universitat Politècnica de Catalunya,  
Campus Sud, Edifici C', C/Pasqual i Vila s/n, Barcelona E-08028, Spain*

<sup>5</sup> *Departament d'Enginyeria Química, EUETIB, Universitat Politècnica de  
Catalunya, Comte d'Urgell 187, 08036, Barcelona, Spain.*

\* Corresponding author: [carlos.aleman@upc.edu](mailto:carlos.aleman@upc.edu)

## ABSTRACT

The interaction between morphine (MO), a very potent analgesic psychoactive drug, and five electroactive polymers, poly(3,4-ethylenedioxythiophene) (PEDOT), poly(3-methylthiophene) (P3MT), polypyrrole (PPy), poly(N-methylpyrrole) (PNMPy) and poly[N-(2-cyanoethyl)pyrrole] (PNCyPy), has been examined using theoretical calculations on model complexes and voltammetric measures considering different pHs and incubation times. Quantum mechanical calculations in model polymers predict that the strength of the binding between the different polymers and morphine increases as follows: PEDOT < PNMPy < PPy << P3MT ≈ PNCyPy. The most relevant characteristic of P3MT is its ability to interact with morphine exclusively through non-directional interactions. On the other hand, the variations of the electroactivity and the anodic current at the reversal potential evidence that the voltammetric response towards the presence of MO is considerably higher for P3MT and PNCyPy than that for the other polymers at both acid (P3MT > PNMPy) and neutral (P3MT ≈ PNCyPy) pHs. Energy decomposition analyses of the interaction of MO with different model polymers indicate that the stronger affinity of MO for P3MT and PNCyPy as compared to PEDOT, PNMPy, and PPy is due to more favorable orbital interactions. These more stabilizing orbital interactions are the result of the larger charge transfer from MO to P3MT and PNCyPy model polymers that takes place because of the higher stability of the single occupied molecular orbital (SOMO) of these model polymers. Therefore, to design polymers with a large capacity to detect MO we suggest looking at polymers with high electron affinity.

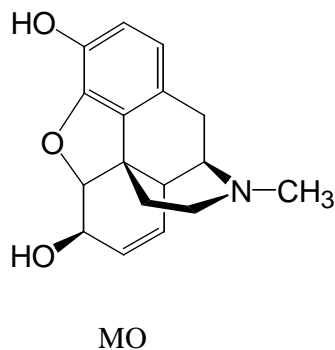
## INTRODUCTION

Because their chemical and physical properties may be tailored over a wide range of characteristics, the use of polymers is finding a permanent place in sophisticated electronic measuring devices such as sensors.<sup>1-5</sup> Among this wide family of organic materials, electroactive polymers (EPs) have emerged as attractive candidates for sensing elements due to its unique electrochemical, electrical and optical properties. Thus, properties of these  $\pi$ -conjugated organic materials have been observed to change at room temperature when they are exposed to low concentrations of chemical species, making EPs useful as sensors of gases,<sup>6-8</sup> metallic ions,<sup>9-12</sup> biomolecules,<sup>14-19</sup> etc, for environmental and clinical monitoring.

To rationalize and complete experimental sensing information, molecular modeling investigations are extremely useful. Within this context, first principle theoretical studies through sophisticated quantum mechanical (QM) calculations are known to be useful tools for quantifying both intramolecular and intermolecular interactions that govern sensor...analyte binding.<sup>20-29</sup> Indeed, such methods provide accurate molecular geometries, give access to the conformational energetic and are able to delineate the sensor...analyte interactions pattern. Indeed, our QM investigations on complexes formed by model EPs and different types of analytes (*e.g.* metallic cations,<sup>24,25</sup> neurotransmitters,<sup>26</sup> DNA bases<sup>27,28</sup> and vapor of solvents<sup>29</sup>) have been devoted to establish a relationship between the experimental sensing information and both the interaction pattern and the binding energies.

We are currently interested in the development of EP-based biosensors to detect certain types of narcotic drugs with clinical applications. Within this specific context, the development of advanced systems to detect morphine (MO; **Scheme 1**), which is the principal active component in opium, is particularly interesting since it is frequently

used in medicine to relieve severe pain of patients. However, this extremely potent analgesic psychoactive drug, which affects drastically the individual abilities of the user, is very toxic in excess or when abused.

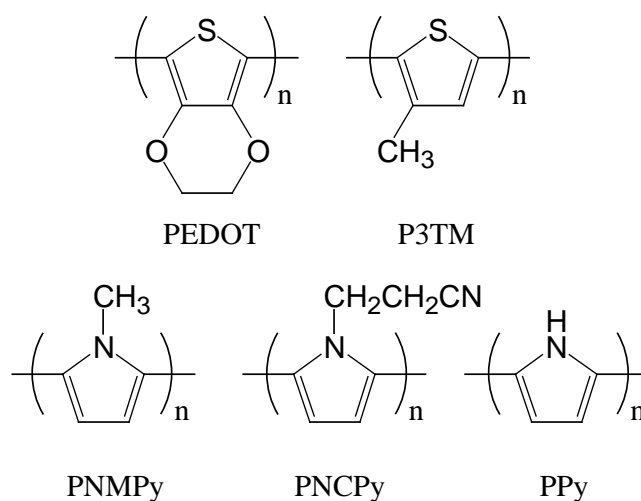


**Scheme 1.** Molecular structure of MO.

Currently, detection of MO in clinical assays is carried out using high-performance liquid chromatography followed by UV spectroscopy<sup>30</sup> and conventional electrochemical methods.<sup>31,32</sup> Recently, the excellent properties of poly(3,4-ethylenedioxythiophene) (Scheme 2), abbreviated PEDOT, were used to propose a more convenient method to detect MO.<sup>33,34</sup> PEDOT and its derivatives were settled among the most successful EPs due to their high electrochemical and environmental stability, high conductivity, high transparency and high biocompatibility.<sup>35-39</sup> Detection of MO with PEDOT was carried out using immobilized molecularly imprinted polymer (MIP) particles, this procedure being successful for drug concentrations ranging from 0.01 to 0.2 mM.<sup>33</sup> More recently, Atta and co-workers<sup>40</sup> investigated the electrochemical determination of MO at PEDOT modified platinum electrodes in presence of sodium dodecyl sulfate. Specifically, the detection procedure proposed by these authors was based on the oxidation of the phenolic group of MO at +0.41 V.

In this work we present a comprehensive detection study based to compare the affinity of five different EPs (Scheme 2) towards MO: PEDOT, poly(3-

methylthiophene) (P3MT), polypyrrole (PPy), poly(N-methylpyrrole (PNMPy) and poly[N-(2-cyanoethyl)pyrrole] (PNCPy). PEDOT has been successfully used to detect specific nucleotide sequences in DNA<sup>18,41</sup> as well as different small biomolecules, including drugs.<sup>42</sup> Comparison between PEDOT and P3MT is expected to provide useful information about the influence of hydrogen bonding interactions in the detection of MO (*i.e.* the oxygen atoms of the dioxane ring in PEDOT repeat unit were found to form strong intermolecular hydrogen bonds<sup>18,27,28,41</sup>). PPy, PNMPy and PNCPy showed sensing abilities for the detection of dopamine that, as MO, presents aromatic and hydroxyl groups.<sup>17,26</sup> Indeed, the sensing ability of these EPs to detect dopamine was found to increase as follows: PPy < PNMPy < PNCPy. Furthermore, a recent study evidenced the high ability of PPy and PNMPy to capture MO molecules and to retain them for a long period.<sup>43</sup>



**Scheme 2:** Molecular structure of the investigated CPs

The present study is based on both theoretical QM calculations and experimental measures to evaluate the intrinsic detection ability of PEDOT, P3MT, PPy, PNMPy and PNCPy. More specifically, QM calculations have been used to provide microscopic

understanding of the non-covalent interactions involved in the interaction between the EPs and MO. For this purpose, the geometry and strength of the binding between each EP and MO have been evaluated using model complexes. Experimental studies to examine the sensing ability of the five EPs have been performed using cyclic voltammetry (CV) considering different pHs and incubation times. QM and CV results have been found to be fully consistent, the experimentally measured ability to detect MO increasing with the predicted binding energy. Finally, interactions have been analyzed by means of energy decomposition analyses at the QM level.

## METHODS

### Computational methods

Calculations were performed using the Gaussian 09 rev. A02 computer program.<sup>44</sup> PEDOT, P3MT, PPy, PNMPy and PNCpy were modeled considering small oligomers containing  $n$  repeat units in the radical cation state ( $n$ -EPs, charge= +1 and spin multiplicity= 2). It is worth noting that the selection of oxidized  $n$ -oligomers was based on our own experimental results (see Results and Discussion section), which indicated that at the detection potential the polymer is oxidized. MO was considered in its neutral form and the molecular geometry used as starting point corresponded to the obtained high resolution X-ray crystallography.<sup>45</sup>

The structure of  $n$ -EPs...MO complexes was determined by full geometry optimization using the UHF formalism combined with the basis set 6-31+G(d,p).<sup>46-48</sup> Harmonic vibrational frequencies were computed to verify the nature of the minimum state of the resulting stationary points. In order to include electron correlation effects in energy estimations, single-point calculations were performed at the UMP2 level<sup>49</sup> using

the 6-31+G(d,p) basis set. The basis set superposition error (BSSE) was corrected using the counterpoise (CP) method.<sup>50</sup>

Binding energies,  $\Delta E_b$ , were estimated as the difference between the total energy of the optimized complex ( $E_{AB}$ ) and the energies of the isolated subsystems with the geometries obtained from the optimization of the complex:

$$\Delta E_{int} = E_{AB} - E_{A(B)} - E_{B(A)} \quad (1)$$

where  $E_{A(B)}$  and  $E_{B(A)}$  refer to energies of the subsystem after correct the BSSE. Electron densities were calculated at the UMP2/6-31+G(d,p) level using the UHF/6-31+G(d,p) geometries –DISPONIBLES, VER AL FINAL SI LA VALE LA PENA INCLUIRLO O NO-.

In addition, with the aim of achieving a better comprehension of the interaction between MO and the different polymers, energy decomposition analysis<sup>51-54</sup> (EDA) were performed on the UHF/6-31+G(d,p) optimized geometries of 3-EPs model polymers by means of the Amsterdam Density Functional package (ADF).<sup>55,56</sup> The EDA has been performed with the TZ2P basis set of Slater type orbitals (STOs)<sup>57</sup> of triple- $\xi$  quality containing two sets of polarization functions. The core shells of carbon, nitrogen, oxygen and sulfur were treated by the frozen-core approximation. Energies were calculated with the generalized gradient approximation (GGA) using the BP86-D functional,<sup>58-61</sup> which includes the dispersion-correction as developed by Grimme<sup>62,63</sup> for a correct treatment of the stacking interactions.

In the EDA, the interaction energy ( $\Delta E_{int}$ ) between the MO and the model polymer is analyzed in the framework of the Kohn–Sham molecular orbital model using a quantitative decomposition of the bond into electrostatic interaction, Pauli repulsion, orbital interactions, and dispersion energy terms represented as:  $\Delta E_{int} = \Delta E_{Pauli} + \Delta V_{elstat} + \Delta E_{oi} + \Delta E_{disp}$ .<sup>51-54</sup> In particular, the orbital interactions component ( $\Delta E_{oi}$ ) accounts for

charge transfer (i.e., donor–acceptor interactions between occupied orbitals on one fragment with unoccupied orbitals of the other) and polarization (empty–occupied orbital mixing on one fragment due to the presence of the other fragment). Finally, Hirshfeld charges were also calculated to analyze the charge transfer between MO and the 3-EPs.<sup>64</sup>

### **Experimental methods**

*Materials.* 3,4-ethylenedioxythiophene (EDOT), 3-methylthiophene (3MT), pyrrole (Py), N-methylpyrrole (NMPy) and N-(2-cyanoethyl)pyrrole (NCPy) monomers and acetonitrile (all analytical reagent grade) were purchased from Aldrich and used as received. Anhydrous LiClO<sub>4</sub>, analytical reagent grade from Aldrich, was stored in an oven at 80 °C before use in the electrochemical trials. MO solution also was purchased from Aldrich, and used as received. TRIS buffer solutions, purchased from Aldrich, were adjusted to different pH values: pH=2 and 7 with HCl (purchased from Panreac), and pH=8.5 with NaOH (purchased from Panreac).

*Preparation.* PEDOT, PPy, PNMPy and PNCPy films were prepared by chronoamperometry (CA) under a constant potential of 1.40 V using polymerization times of  $\theta = 300, 600, 600$  and 1200 s, respectively. P3MT was obtained using recurrent potential pulses (RPP) of 50 s between 0.70 and 1.70 V, details on the experimental conditions being reported previously.<sup>65</sup> These synthetic procedures allowed us to obtain films of similar thickness in all cases (i.e. 2.1–2.6  $\mu\text{m}$  as determined by optical profilometry using a WYKO 9300NT optical profiler - Veeco, Plainview, NY). Anodic electropolymerization and electrochemical experiments were performed on a VersaStat II potentiostat-galvanostat using a three-electrode two-compartment cell under nitrogen atmosphere at 25 °C. For the polymerizations by CA the anodic compartment was filled

with 40 mL of a 10 mM monomer solution in acetonitrile containing 0.1 M LiClO<sub>4</sub> as supporting electrolyte, while the cathodic compartment contained 10 mL of the same electrolyte solution. P3MT films were produced using 0.2 M monomer acetonitrile solutions with 0.1 M LiClO<sub>4</sub>. Platinum sheets of 1 cm<sup>2</sup> area were employed as working electrodes, whereas counter electrodes were made of steel AISI 316 in all cases. The reference electrode was an Ag|AgCl electrode containing a KCl saturated aqueous solution.

*Electrochemical measurements for detection of MO.* Electrochemical detection was carried out by CV using an PGSTAT302N AUTOLAB potentiostat-galvanostat (Ecochimie, The Netherlands) equipped with the ECD module to measure very low current densities (100 μA-100 pA), which was connected to a PC computer controlled through the NOVA 1.6 software. Electrochemical experiments were performed at room temperature using TRIS buffer solutions adjusted to pH = 2, 7 and 8.5. It should be noted that, although the useful buffer range of TRIS solutions is 7-9, the pH of the solutions adjusted to 2 will not be altered by oxidation and reduction processes carried out in this study because of the used potentials. The glass cell used for detection assays was equipped with saturated Ag|AgCl as reference electrode and platinum (Pt) wire as counter electrode. Voltammograms were recorded in the potential range from -0.50 to 1.60V at a scan rate of 50 mV·s<sup>-1</sup> unless other scan rate is explicitly specified. Before to record the voltammograms, EP films deposited on Pt were subjected to the following experimental conditions: (a) immersion at room temperature in TRIS buffer solutions at pH= 2, 7 and 8.5 during 3 h, 12 h and 24 h (*blank samples*); and (b) incubation at room temperature during 3, 12 and 24 h in 3.5 mM MO TRIS buffer solutions at pH= 2, 7 and 8.5 (*incubated samples*).

## RESULTS AND DISCUSSION

### Theoretical calculations: Interaction patterns and binding energies

The interaction between the EPs and MO was modeled using a build-up approach that was previously used to investigate the interaction of dopamine with both PNMPy and PNCPy.<sup>26</sup> For this purpose,  $n$ -EP...MO model complexes of growing  $n$ , where  $n$  indicates the number of repeat units, were selectively built. More specifically, the interaction of complexes with  $n=1$  was examined in a first stage, the resulting complexes being used to construct the starting structures for 2-EP...MO. Finally, the starting arrangements of 3-EP...MO were constructed using the optimized geometries of 2-EP...MO. Analysis of the results has been focused on 3-EP...MO complexes, which are the most representative.

Geometry optimizations of 12 starting structures for 1-EDOT...MO led to 8 different arrangements, which were categorized in six different groups according to the interaction patterns. The number of starting structures was increased to 20 for all the remaining 1-EP...MO complexes, the number of different arrangements derived from their optimization being 8, 8, 8 and 8 for 1-3MT...MO, 1-Py...MO, 1-NMPy...MO and 1-NCPy...MO, respectively. According to the interaction pattern, the optimized geometries of 1-3MT, 1-Py and 1-NMPy complexes were classified in 6 groups while those of 1-NCPy...MO were categorized in 8 groups. The most stable structure of each group was used to construct the starting structures of 2-EP...MO complexes by adding a new repeat unit. After geometry optimization, 5, 4, 5, 4 and 6 different structures were obtained for 2-EDOT...MO, 2-3MT...MO, 2-Py...MO, 2-NMPy...MO and 2-NCPy...MO complexes, respectively. As occurred above, the structures obtained for 2-EP...MO were used to build the starting arrangement of 3-EP...MO complexes. For each 3-EP...MO complex, optimized structures with different interaction patterns and

relative energies ( $\Delta E$ ) lower than 3.0 kcal/mol with respect to the most stable one were the only considered for analysis. Thus, the number of structure that fulfilled such requirements was 4, 2, 4, 3, and 1 for 3-EDOT...MO, 3-3MT...MO, 3-Py...MO, 3-NMPy...MO and 3-NCPy...MO complexes, which are depicted in **Figure 1**. Both  $\Delta E$  and  $\Delta E_b$  values for each complex are listed in **Table 1**.

The four 3-EDOT...MO structures (**Figure 1a**) are within a  $\Delta E$  interval of only 0.8 kcal/mol. As it can be seen, all four structures are stabilized by C–H...O interactions while, amazingly, no conventional O–H...O hydrogen bond is detected. In addition, the lowest energy structure (**3-EDOTa**) shows a  $\pi$ -stacking interaction with the two aromatic rings arranged perpendicularly (*i.e.* T-shaped disposition). The remaining 3 structures (**3-EDOTa-c**) only differ in the relative orientation of the two molecules, which explains their resemblance in terms of  $\Delta E$ . The strength of the binding is similar for the four structures with  $\Delta E_b$  values ranging from -10.5 to -12.3 kcal/mol. The two structures obtained for 3-3MT...MO, **3-3MTa** and **3-3MTb**, are separated by 1.7 kcal/mol. Although these two structures are mainly stabilized by non-specific intermolecular interactions, the  $\Delta E_b$  values, -48.2 and **-47.1** kcal/mol, are significantly lower than those obtained for 3-EDOT...MO structures. This should be attributed to the fact that the contact surface between the two molecules is larger in 3-3MT...MO than in 3-EDOT...MO, enhancing the contribution of the electrostatic interactions provoked by the positive charge localized in the 3-3MT oligomer.

**Figure 1c** displays the four structures obtained for 3-Py...MO, which are comprised within a  $\Delta E$  interval of 2.7 kcal/mol. The lowest energy structure (**3-Pya**) is stabilized by a N–H...O hydrogen bond and a C–H...O interaction, which involve the same hydroxyl group of MO. Although the nature of the intermolecular interactions in the next structure (**3-Pyb**), which is destabilized by only 0.3 kcal/mol, is similar to those of

**3-Pya**, some clear differences are identified. The most relevant ones can be summarized as follows: 1) the relative orientation of the two interacting molecules change with respect to **3-Pya**; 2) the MO hydroxyl group involved in the intermolecular interactions of the two structures is different; and 3) the oxygen of MO in **3-Pyb** forms one N–H···O hydrogen bond and two C–H···O interactions rather than one interaction of each type, as in **3-Pya**. The third structure (**3-Pyc**) essentially differs from the lowest energy one in the relative orientation of the two fragments as well as in the fact that intermolecular interactions involve two oxygen atoms of MO. Finally, the fourth structure (**3-Pyd**) presents a  $\pi$ -stacking, in addition to the N–H···O hydrogen bond and the C–H···O interaction. In spite of the  $\pi$ -stacking is not present in the three previous structures, **3-Pyd** is disfavored by 2.1 kcal/mol with respect to **3-Pyc**. The  $\Delta E_b$  of these structures (Table 1) ranges from -25.2 kcal/mol (**3-Pya**) to -18.2 kcal/mol (**3-Pyb**) indicating that MO interacts more favorably with PPy than with PEDOT but less favorably than with P3MT.

Three different structures separated by a  $\Delta E$  interval of 1.4 kcal/mol have identified for 3-NMPy···MO. The two structures of lowest energy are practically isoenergetic (**3-NMPya** and **3-NMPyb** in Figure 1d), being stabilized by C–H···O interactions. Although the number of such interactions is higher for **3-NMPya** than for **3-NMPyb** (*i.e.* 4 and 2, respectively), the strength of such interactions is higher for the latter than for the former (*i.e.* H···O distances are larger for **3-NMPya** than for **3-NMPyb**). This feature explains not only their isoenergetic behavior but the corresponding  $\Delta E_b$  values (Table 1). Although the third structure, **3-NMPyc**, also presents C–H···O interactions, the geometric distortions associated to the binding process provokes a small energy penalty (*i.e.* 1.7 kcal/mol). Results indicate that the affinity of PNMPy towards MO is higher than that of PEDOT but lower than those of PPy and, especially, P3MT.

Finally, the 3-NCPy...MO only presented one structure within a  $\Delta E$  interval of 3.0 kcal/mol (3-NCPya in Figure 1e). This structure, which shows a  $\Delta E_b$  of -50.9 kcal/mol, is stabilized by a strong O-H...N hydrogen bond, with a H...O distance of only 1.87 Å, and a C-H...N interaction. Comparison of  $\Delta E_b$  values listed in Table 1 allows us to predict that the strength of the binding between the studied EPs and MO increases as follows: PEDOT < PNMPy < PPy << P3MT  $\approx$  PNCPy. As it can be seen, these EPs can be categorized in two classes depending on their affinity towards MO: a) those with  $\Delta E_b$  values lower than  $\sim -25.0$  kcal/mol; and b) those with  $\Delta E_b$  values about  $\sim -50.0$  kcal/mol. Unexpectedly, polymers with highest tendency to act as hydrogen bonding acceptor (*i.e.* the oxygen atoms of PEDOT) and donor (*i.e.* the N-H of PPy) belong to the former class.

With the aim to understand this surprising trend, we have performed an EDA of the interaction between MO and 3-EPs model polymers for the most stable structures in each case. From the values in Table 2 we find that the main factor determining the different interaction energies is the orbital interaction component. Those polymers that present the strongest interaction, PNCPy and P3MT, are the ones with the most stabilizing orbital interaction term (from -27.8 to -44.3 kcal mol<sup>-1</sup>). On the other hand, the rest of the systems, which present a weaker interaction, have also much less stabilizing  $\Delta E_{oi}$  values (from -5.0 to -12.1 kcal mol<sup>-1</sup>). The rest of terms of the EDA analysis do not play a determinant role. Hirshfeld charges of MO were calculated to discuss the origin of the different  $\Delta E_{oi}$  values. Let us remind that initially MO is neutral, whereas the model polymer is charged +1 as a doublet spin state due to its unpaired electron, which is located in a single occupied molecular orbital (SOMO). The Hirshfeld charges of MO in Table 2 show a clear difference between the strongly bound 3-PEs models of PNCPy and P3MT and the rest, as for the former a transfer of almost

one electron from MO to the polymer is observed with positive charges on MO of 0.74 e for **3-MT** and 0.91 e for **3-NCPy**. On the other hand, for the weaker interacting polymers we find that MO keeps almost neutral and uncharged. The charge transfer in MO···PNCPy and MO···P3MT is favored by the lower energy of their SOMOs as can be seen Table 2 that gathers the relative energies of the SOMOs of the 3-PEs analyzed. The higher charge transfer in 3-PEs models of PNCPy and P3MT justify the more stabilizing  $\Delta E_{oi}$  component. Therefore to design polymers that improve detection of MO, the determinant factor that one should look at is the energy of the SOMO. Polymers with more stable SOMOs have a high capacity to accept electrons and will result in improved interactions with MO.

In the next section, the interaction between MO and the polymers will be analyzed through voltammetric measures to confirm the above discussed quantum chemical calculations.

### **Electrochemical behavior of the CPs**

Many EPs prepared in aqueous solution are not stable at potentials higher than  $\sim 1.1$  V,<sup>43,66,67</sup> which represents a serious limitation. In order to overcome it, EPs were generated in acetonitrile, which allowed us to ensure the stability of this material in the whole potential range used in this study (*i.e.* between  $-0.50$  and  $1.60$  V). As the detection assays have been performed considering different incubation times in TRIS solutions acid, neutral and basic pHs (see next sub-section), in this sub-section we examine the electrochemical behavior of the five EPs in absence of MO but using the above mentioned experimental conditions.

**Figure 2** compares the control voltammograms of fresh modified electrodes before any incubation process (*i.e.* Pt electrodes coated with the EPs after their immediate

immersion in TRIS solutions with pHs adjusted at 2, 7 and 8.5) with that of Pt. The electrochemical response of all the EPs, which has been characterized by both the ability to store charge (electroactivity) and the anodic current at the highest potential ( $j_{max}$ ), depends on the pH. As it can be seen, the electroactivity is significantly higher for P3MT than for the other CPs at pH= 2 and 7 (*i.e.* approximately 64-67% and 68-73% at acid and neutral pH, respectively). Interestingly, the electroactivity decreases in all cases with exception of PEDOT when the pH increases from 7 to 8.5, this reduction ranging from 31% (PCNPy) to 60% (P3MT). In the case of PEDOT the electroactivity increases 82%. The same behavior is observed for  $j_{max}$ , which for P3MT is higher than 60 mA/cm<sup>2</sup> at pH= 2 and 7 and decreases to 26 mA/cm<sup>2</sup> at pH= 8.5. This reduction is less pronounced for the rest of the EPs (*i.e.* typically from ~25 to ~10 mA/cm<sup>2</sup>), an exception being observed for PEDOT (*i.e.*  $j_{max}$  increases from 34 to 38 mA/cm<sup>2</sup> with the pH).

### **Voltammetric detection of morphine**

Control voltammograms of blank and incubated samples (*i.e.* those immersed in TRIS solution and MO-containing TRIS solution, respectively) were recorded considering immersion times of 3, 12 and 24 h and pHs of 2, 7 and 8.5. **Figure 3** represents the control voltammograms recorded for systems immersed in solutions with pH= 2. As it can be seen, the largest difference between blank and incubated samples in this acid environment occurs for P3TM and PNCPy, independently of the immersion time. However, differences between blank and incubated samples of some other EPs are also clearly appreciable for specific immersion times. The ability to detect MO of the five EPs has been quantified by considering, for each immersion time, the difference of the electroactivity and  $j_{max}$  values between the incubated and blank samples ( $\Delta Q$  in % and

$\Delta j_{\max}$  in mA/cm<sup>2</sup>, respectively). More specifically, the EP has been considered as appropriated only when the two following conditions are fulfilled simultaneously: (i)  $\Delta Q \geq 125\%$  or  $\Delta Q \leq 75\%$ ; and (ii)  $\Delta j \geq |10|$  mA/cm<sup>2</sup> (*i.e.* MO provokes significant changes in anodic and cathodic areas as well in the anodic density at the reversal potential). Results, which are depicted in Figures 4a and 4b, indicate that the ability to detect MO of the different EPs at pH= 2 decreases as follows: P3MT > PNCPy >> PPy > PNMPy. Results for PEDOT are completely inappropriate for all immersion times since the change in the voltammetric response of this EP is very weak.

Control voltammograms of samples immersed in solutions with pH= 7 are displayed in Figure 5 while the variation of  $\Delta Q$  and  $\Delta j_{\max}$  with the immersion time are represented in Figures 4c and 4d, respectively. Visual inspection of the voltammograms obtained indicates that the results obtained at pH= 7 are similar to those achieved in acid environment for P3MT and PNCPy. Thus, such two EPs exhibit the highest variation in the voltammetric response, independently of the immersion time. However, some changes are identified for PEDOT and PPy. More specifically, the detection ability of the former exhibits an improvement with respect to pH= 2, while the behavior of the latter becomes clearly worse. Considering the criteria used above, the response of EPs towards MO can be described as follows: P3MT  $\approx$  PNCPy >> PEDOT. At neutral pH the response of PPy and PNMPy is not appropriated for MO detection.

Finally, the cyclic voltammograms recorded in solutions with pH= 8.5 (Figure 6) as well as of  $\Delta Q$  and  $\Delta j_{\max}$  values (Figures 4e and 4f, respectively) evidence that the response of all EPs towards MO is weak or even very weak. This has been attributed to the competition between the hydroxyl and other negatively charged species, especially dopant anions.

### Stability for the voltammetric detection of morphine

The electrochemical stability quantifies how the ability to store charge a material decreases upon consecutive oxidation-reduction cycles. This property has been used to evaluate how repetitive is the measure of electrochemical parameters for the detection of MO without significant detriment in the intensity of the signals. The effect of consecutive oxidation-reduction cycles on the voltammetric response of EPs in absence and presence of MO was examined by considering P3MT (incubation time 3h and 12h for pH= 2 and 7, respectively) and PNCPy (incubation time 12h and 24h for pH= 2 and 7, respectively), which were the more efficient EPs for sensing at acid and neutral pHs. **Figure 7** represents the voltammograms of blank and incubated samples after 10 consecutive redox cycles. As it can be, seen the largest differences in terms of  $\Delta Q$  and  $\Delta j_{\max}$  at both pH= 2 and 7 are detected for PNCPy. More specifically, the  $\Delta j_{\max}$  measured for P3MT at pH=2 and 7 is -2.1 and 3.7 mA/cm<sup>2</sup>, respectively, which represent a very drastic reduction with respect to the values derived from the first control voltammograms (*i.e.* 157 and 26.1 mA/cm<sup>2</sup>, respectively). However, the  $\Delta j_{\max}$  determined for PNCPy after 10 cycles, 10.1 and 5.5 mA/cm<sup>2</sup> at pH= 2 and 7, respectively, are relatively close to those obtained in the first control voltammogram (*i.e.* 17.3 and 19.3 mA/cm<sup>2</sup>, respectively). Inspection of  $\Delta Q$  shows similar trends, redox cycles provoking large and moderate reductions in the difference of electroactivities for P3MT and PNCPy, respectively. The overall of these results indicate that the latter EP is the most stable for the voltammetric detection of MO.

### CONCLUSIONS

The ability of five different EPs to interact with MO has been evaluated using QM and voltammetric detection assays. QM calculations on model complexes indicate that

the affinity of all these EPs towards morphine, with exception of that of P3MT, is dominated by a combination of different directional interactions: C–H···O (PEDOT, PPy and PNMPy),  $\pi$ -stacking (PEDOT and PPy), N–H···O (PPy), O–H···N (PNCPy) and C–H···N (PNCPy). In contrast, P3MT only interacts with MO through non-directional van der Waals interactions. Calculations predict that the strength of the interaction between each EP and MO decreases as follows: **PNCPy  $\approx$  P3MT**  $\gg$  PPy  $>$  PNMPy  $>$  PEDOT. Cyclic voltammetry assays are fully consistent with these results at acid and neutral pHs. Thus, the MO-induced changes in both the electroactivity and the anodic current at the reversal potential are larger for P3MT and PNMPy than for PPy, PNMPy and PEDOT at pH= 2 (P3MT  $>$  PNCPy) and pH= 7 (P3MT  $\approx$  PNCPy). In contrast, the voltammetric behavior of all investigated polymers is similar in presence and absence of MO at pH= 8.5. Although the responses of P3MT and PNCPy for the voltammetric detection of MO are clearly better than those of the other EPs, the stability of such responses is higher for PNMPy than for P3MT. **Finally, energy decomposition analyses show that the stronger interaction of MO with P3MT and PNCPy as compared to the other studied polymers is due to the higher stability of their SOMOs, which favors the transfer of charge from MO to the polymers leading to stronger orbital interactions. This allows us to conclude that to design new polymers with a larger capacity of detecting morphine we should focus on the energy of its SOMO and choose those polymers with large electron affinity.**

## ACKNOWLEDGEMENTS

This work has been supported by MICINN and FEDER funds (project **numbers** MAT2012-34498, **CTQ2011-23156/BQU** and **CTQ2011-25086/BQU**), by the DIUE of the Generalitat de Catalunya (contracts **numbers** 2009SGR925, **2009SGR528**,

2009SGR637 and XRQTC) and Cátedra Applus (UPC). E.C.-M. and B. T. D. are thanked to the MICINN by their FPI grants. Support for the research of C.A. and M. S. was received through the prize “ICREA Academia” for excellence in research funded by the Generalitat de Catalunya.

## REFERENCES

- [1] S. Cosnier, *Electroanalysis* 17 (2005) 1701-1705.
- [2] B. Adhikari, S. Majumdar, *Prog. Polym. Sci.* 29 (2004) 699-766.
- [3] B. D. Malhotra, A. Chaubey, S. P. Singh, *Anal. Chim. Acta* 578 (2006) 59-74.
- [4] L. A. Terry, S. F. White, L. J. Tigwell, *J. Agric. Food Chem.* 53 (2005) 1309-1319.
- [5] T. G. Drummond, M. G. Hill, J. K. Barton, *Nat. Biotechnol.* 21 (2003) 1192-1199.
- [6] S. J. Marsella, P. J. Carroll, T. M. Swager, *J. Am. Chem. Soc.* 117 (1995) 9832-9841.
- [7] L. Torsi, M. Pezzuto, P. Siciliano, R. Rella, L. Sabbatini, L. Valli, P. Zambonin, *Sens. Actuators* 48 (1998) 362-367.
- [8] K. Ogura, T. Saino, M. Nakayama, H. Shiigi, *J. Mat. Chem.* 7 (1997) 2363-2366.
- [9] M. J. Marsella, T. M. Swager, *J. Am. Chem. Soc.* 115 (1993) 12214-12215.
- [10] P. Bäuerle, S. Scheib, *Adv. Mater.* 5 (1993) 848-853.
- [11] B. Joussetme, P. Blanchard, E. Levillain, J. Delaunay, M. Allain, P. Richomme, D. Rondeau, N. Gallego-Planas, J. Roncali, *J. Am. Chem. Soc.* 125 (2003) 1363-1370.
- [12] J. Casanovas, J. Preat, D. Zanuy, C. Alemán, *Chem. Eur. J.* 15 (2009) 4676-4684.
- [13] B. S. Gaylord, A. J. Heeger, G. Bazan, *Proc. Natl. Acad. Sci. USA* 99 (2002) 10954-10957.
- [14] H.-A. Ho, M. Bossinot, M. G. Bergeron, G. Corbeil, K. Doré, B. Boudreau, M. Leclerc, *Angew. Chem. Int. Ed.* 41 (2002) 1548-1551.

- [15] A. Azioune, M. M. Chehimi, B. Miksa, T. Basinska, S. Slonkowski, *Langmuir* 18 (2002) 1150-1150.
- [16] G. G. Wallace, L. A. P. Kane-Maguire, *Adv. Mater.* 14 (2002) 953-960.
- [17] M. Martí, G. Fabregat, F. Estrany, C. Alemán, E. Armelin, *J. Mat. Chem.* 20 (2010) 10652-10660.
- [18] B. Teixeira-Dias, D. Zanuy, J. Poater, M. Solà, F. Estrany, L. J. del Valle, C. Alemán, *Soft Matter* 7 (2011) 9922-9932.
- [19] B. Teixeira-Dias, L. J. del Valle, F. Estrany, E. Armelin, R. Oliver, C. Alemán, *Eur. Polym. J.* 44 (2008) 3700-3707.
- [20] De Vivo, M. Bridging Quantum Mechanics and Structure-Based Drug Design. *Front. Biosci.* 2011, 16, 1619-1633.
- [21] Menikarachchi, L. C.; Gascón, J. A. QM/MM Approaches in Medicinal Chemistry Research. *Curr. Top. Med. Chem.* 2010, 10, 46–54.
- [22] J. P. Cerón Carrasco, D. Jacquemin, J. Graton, S. Thany, J. L. Le Questel, *J. Phys. Chem. B*, **2013**, **117**, 3944-3953.
- [23] J. G. Lee, C. Sagui and C. Roland, *J. Phys. Chem. B*, **2005**, 109, 20588-20596.
- [24] J. Casanovas, J. Preat, D. Zanuy and C. Alemán, *Chem. Eur. J.*, **2009**, **15**, 4676-4684.
- [25] D. Zanuy, J. Preat, E. A. Perpète and C. Alemán, *J. Phys. Chem. B*, **2012**, **116**, 4575-4584.
- [26] G. Fabregat, E. Córdova-Mateo, E. Armelin, O. Bertran and C. Alemán, *J. Phys. Chem. C*, **2011**, **115**, 14933-14941.
- [27] C. Alemán, B. Teixeira-Dias, D. Zanuy, F. Estrany, E. Armelin, L. J. del Valle, *Polymer*, **2009**, **50**, 1965-1974.
- [28] D. Zanuy and C. Alemán, *J. Phys. Chem. B*, **2008**, **112**, 3222-3230.

- [29] D. Aradilla, F. Estrany and C. Alemán, *RSC Adv.*, **2013**, 3, 20545-20558.
- [30] G. Chari, A. Gulati, R. Bhat, I. R. Tebbett, *J. Chromatogr.* 571 (1991) 263-270.
- [31] J. E. Wallace, S. C. Harris, M. W. Peek, *Anal. Chem.* 52 (1980) 1328-1330.
- [32] W. J. Liaw, S. T. Ho, J. J. Wang, O. Y. P. Hu, J. H. Li, *J. Chromatogr. B* 714 (1998) 237-245.
- [33] K.-C. Ho, W.-M. Yeh, T.-S. Tung, J.-Y. Liao, *Anal. Chim. Acta* 542 (2005) 90-96.
- [34] C.-H. Weng, W.-M. Yeh, K.-C. Ho, G.-B. Lee, *Sens. Actuators B* 121 (2007) 576-582.
- [35] L. B. Goenendaal, F. Jonas, D. Freitag, H. Pielartzik, J. R. Reynolds *Adv. Mater.* 12 (2000) 481-494.
- [36] Q. Pei, G. Zuccarello, M. Ahlskog, O. Inganäs, *Polymer* 35 (1994) 1347-1351.
- [37] D.-H. Han, J.-W. Kim, S.-M. Park, *J. Phys. Chem. B* 110 (2006) 14874-14880.
- [38] K. E. Aasmundtveit, E. J. Samuelsen, O. Inganäs, L. A. A. Pettersson, T. Johansson, S. Ferrer, *Synth. Met.* 113 (2000) 93-97.
- [39] L. J. del Valle, F. Estrany, E. Armelin, R. Oliver, C. Alemán, *Macromol. Biosci.* 11 (2008) 1144-1151.
- [40] N. F. Atta, A. Galal, R. A. Ahmed, *Electroanalysis* 23 (2011) 737-746.
- [41] D. Zanuy, B. Teixeira-Dias, L. J. del Valle, J. Poater, M. Solà and C. Alemán, *RSC Adv.* **2013**, 3, 2639–2649.
- [42] N. Rozlosnik, *Anal. Bioanal. Chem.* 395 (2009) 637-645.
- [43] B. Teixeira-Dias, C. Alemán, F. Estrany, D. S. Azambuja, E. Armelin, *Electrochim. Acta*, 2013, **56**, 5836-5843.
- [44] Gaussian 09, Revision A.02, M. J. Frisch, G. W. Trucks, H. B. Schlegel, G. E. Scuseria, M. A. Robb, J. R. Cheeseman, G. Scalmani, V. Barone, B. Mennucci, G. A. Petersson, H. Nakatsuji, M. Caricato, X. Li, H. P. Hratchian, A. F. Izmaylov, J. Bloino,

G. Zheng, J. L. Sonnenberg, M. Hada, M. Ehara, K. Toyota, R. Fukuda, J. Hasegawa, M. Ishida, T. Nakajima, Y. Honda, O. Kitao, H. Nakai, T. Vreven, J. A. Montgomery, Jr., J. E. Peralta, F. Ogliaro, M. Bearpark, J. J. Heyd, E. Brothers, K. N. Kudin, V. N. Staroverov, R. Kobayashi, J. Normand, K. Raghavachari, A. Rendell, J. C. Burant, S. S. Iyengar, J. Tomasi, M. Cossi, N. Rega, J. M. Millam, M. Klene, J. E. Knox, J. B. Cross, V. Bakken, C. Adamo, J. Jaramillo, R. Gomperts, R. E. Stratmann, O. Yazyev, A. J. Austin, R. Cammi, C. Pomelli, J. W. Ochterski, R. L. Martin, K. Morokuma, V. G. Zakrzewski, G. A. Voth, P. Salvador, J. J. Dannenberg, S. Dapprich, A. D. Daniels, O. Farkas, J. B. Foresman, J. V. Ortiz, J. Cioslowski, and D. J. Fox, Gaussian, Inc., Wallingford CT, 2009.

[45] Gylbert, L. *Acta Crystallogr. B* **1973**, *29*, 1630-1635.

[46] Hariharan, P. C.; Pople, J. A. *Theor Chim Acta* **1973**, *28*, 213-222.

[47] Petersson, G. A.; Al-Laham, M. A. *J Chem Phys* **1991**, *94*, 6081-6090.

[48] Frisch, M. J.; Pople, J. A.; Binkley, J. S. *J Chem Phys* **1984**, *80*, 3265-3269.

[49] Moller, C.; Plesset, M. S. *Phys Rev* **1934**, *46*, 618-622.

[50] Boys, S. F.; Bernardi, F. *Mol Phys* **1970**, *19*, 553-566.

[51] K. Morokuma, *Acc. Chem. Res.*, 1977, *10*, 294-300.

[52] K. Kitaura and K. Morokuma, *Int. J. Quantum Chem.*, 1976, *10*, 325-340.

[53] T. Ziegler and A. Rauk, *Theor. Chim. Acta*, 1977, *46*, 1-10.

[54] T. Ziegler and A. Rauk, *Inorg. Chem.*, 1979, *18*, 1755-1759.

[55] G. Te Velde, F. M. Bickelhaupt, E. J. Baerends, C. Fonseca Guerra, S. J. A. van Gisbergen, J. G. Snijders and T. Ziegler, *J. Comput. Chem.*, 2001, *22*, 931-967.

[56] C. Fonseca Guerra, J. G. Snijders, G. te Velde and E. J. Baerends, *Theor. Chem. Acc.*, 1998, *99*, 391-403.

[57] J. G. Snijders, P. Vernooijs and E. J. Baerends, *At. Data Nucl. Data*

Tables, 1981, 26, 483–509.

[58] J. P. Perdew, K. Burke and M. Ernzerhof, *Phys. Rev. Lett.*, 1996, 77, 3865–3868.

[59] J. P. Perdew, K. Burke and Y. Wang, *Phys. Rev. B: Condens. Matter*, 1996, 54, 16533–16539.

[60] A. D. Becke, *Phys. Rev. A* 1988, 38, 3098-3100.

[61] J. P. Perdew, *Phys. Rev. B* 1986, 33, 8822-8824.

[62] S. Grimme, *J. Comput. Chem.*, 2004, 25, 1463–1473; S. Grimme, *J. Comput. Chem.*, 2006, 27, 1787–1799.

[63] S. Grimme, J. Anthony, S. Ehrlich, H. Krieg, *J. Chem. Phys.* 2010, 132, 154104.

[64] F. L. Hirshfeld, *Theor. Chim. Acta* 1977, 44, 129-138.

[65] C. Ocampo, E. Armelin, F. Estrany, L. J. del Valle, R. Oliver, F. Sepulcre and C. Alemán, *Macromol. Mater. Eng.* **2007**, 292, 85-94.

[66] Aradilla, D.; Azambuja, D.; Estrany, F.; Casas, M. T.; Ferreira, C. A.; Alemán, C. *J. Mat. Chem.* **2012**, 22, 13110.

[67] Aradilla, D.; Estrany, F.; Azambuja, D. S.; Casas, M. T.; Puiggali, J. ; Ferreira, C. A.; Alemán, C. *Eur. Polym. J.* **2010**, 46, 977-983.

## CAPTIONS TO FIGURES

**Figure 1.** Geometries of the (a) 3-EDOT...MO, (b) 3-3MT...MO, (c) 3-Py...MO, (d) 3-NMPy...MO and (e) 3-NCPy...MO complexes with  $\Delta E < 3$  kcal/mol derived from QM calculations. C–H...O and C–H...N interactions are indicated by pink lines, aromatic...aromatic staking by yellow lines and N–H...O hydrogen bonds by green lines. The H...O, H...N and aromatic...aromatic (centers of masses) distances are displayed in Å.

(#En aquesta figura cal canviar les etiquetes: 3EDOT per 3-EDOT, etc.)

**Figure 2.** Control voltammograms for the oxidation of Pt coated with P3MT, PEDOT, PPy, PNMPy and PNCPy in TRIS solutions with pH= (a) 2, (b) 7 and (c) 8.5. The voltammogram recorded for the uncoated Pt electrode has been included for comparison. Initial and final potentials: -0.50 V; reversal potential: 1.60 V; scan rate: 50 mV·s<sup>-1</sup>.

**Figure 3.** Control voltammograms for the oxidation of Pt coated with P3MT (a), PEDOT (b), PPy (c), PNMPy (d) and PNCPy (e) in TRIS (solid lines) and MO-containing TRIS (dashed lines) solutions at pH= 2 and incubation times of 3, 12 and 24 h.

**Figure 4.** Difference between the incubated and blank samples in terms of electroactivity,  $\Delta Q$  in % (left), and the current density at the reversal potential  $\Delta j_{\max}$  in mA/cm<sup>2</sup> (right) for the five studied EPs at pH= (a) 2, (b) 7 and (c) 8.5.

**Figure 5.** Control voltammograms for the oxidation of Pt coated with P3MT (a), PEDOT (b), PPy (c), PNMPy (d) and PNCPy (e) in TRIS (solid lines) and MO-containing TRIS (dashed lines) solutions at pH= 7 and incubation times of 3, 12 and 24 h.

**Figure 6.** Control voltammograms for the oxidation of Pt coated with P3MT (a), PEDOT (b), PPy (c), PNMPy (d) and PNCPy (e) in TRIS (solid lines) and MO-containing TRIS (dashed lines) solutions at pH= 7 and incubation times of 3, 12 and 24 h.

**Figure 7.** Control voltammograms for Pt coated with P3MT (a) and PNCPy (b) after ten consecutive oxidation-reduction cycles in TRIS (solid lines) and MO-containing TRIS (dashed lines) solutions at pH= 2 and 7 and the indicated incubation times.

**Table 1.** Relative energy ( $\Delta E$ ; in kcal/mol) and binding energy after correct the basis set superposition error ( $\Delta E_b$ ; in kcal/mol) for 3-EDOT...MO, 3-3MT...MO, 3-Py...MO, 3-NMPy...MO and 3-NCPy...MO complexes (see **Figure 1**) at the UMP2/6-31+G(d,p) level.

	$\Delta E$	$\Delta E_b$		$\Delta E$	$\Delta E_b$
<b>3-EDOTa</b>	0.0	-11.1	<b>3-Pya</b>	0.0	-25.2
<b>3-EDOTb</b>	0.1	-10.9	<b>3-Pyb</b>	0.3	-18.2
<b>3-EDOTc</b>	0.5	-10.5	<b>3-Pyc</b>	0.6	-19.1
<b>3-EDOTd</b>	0.8	-12.3	<b>3-Pyd</b>	2.7	-19.0
<b>3-3MTa</b>	0.0	-48.2	<b>3-NMPya</b>	0.0	-13.2
<b>3-3MTb</b>	1.7	-47.1	<b>3-NMPyb</b>	0.1	-14.4
			<b>3-NMPyc</b>	1.4	-14.1
			<b>3-NCPya</b>	0.0	-50.9

**Table 2.** Energy decomposition analysis terms and relative energy of the SOMO with respect to that of **3-CPy**, in kcal mol<sup>-1</sup>, and Hirshfeld charges of MO.

	$\Delta E_{\text{Pauli}}$	$\Delta V_{\text{elstat}}$	$\Delta E_{\text{oi}}$	$\Delta E_{\text{disp}}$	$\Delta E_{\text{int}}$	$\Delta E_{\text{SOMO}}$	q(MO)
<b>3-3MTa</b>	4.70	0.45	-27.85	-9.57	-32.27	11.92	0.74
<b>3-3MTb</b>	4.40	0.39	-31.71	-7.84	-34.75	7.53	0.79
<b>3-NCPya</b>	16.10	-14.68	-44.34	-6.17	-49.09	0.00	0.91
<b>3-EDOTa</b>	5.66	-7.36	-4.96	-8.19	-14.85	48.32	0.07
<b>3-EDOTb</b>	4.68	-7.93	-5.33	-4.29	-12.88	48.95	0.02
<b>3-NMPya</b>	5.81	-9.75	-6.65	-5.56	-16.14	39.53	0.04
<b>3-NMPyb</b>	6.13	-10.53	-6.54	-6.02	-16.96	39.53	0.02
<b>3-Pya</b>	11.25	-18.13	-12.10	-10.46	-29.45	33.26	0.06
<b>3-Pyb</b>	11.53	-15.96	-11.36	-6.76	-22.55	33.89	0.05

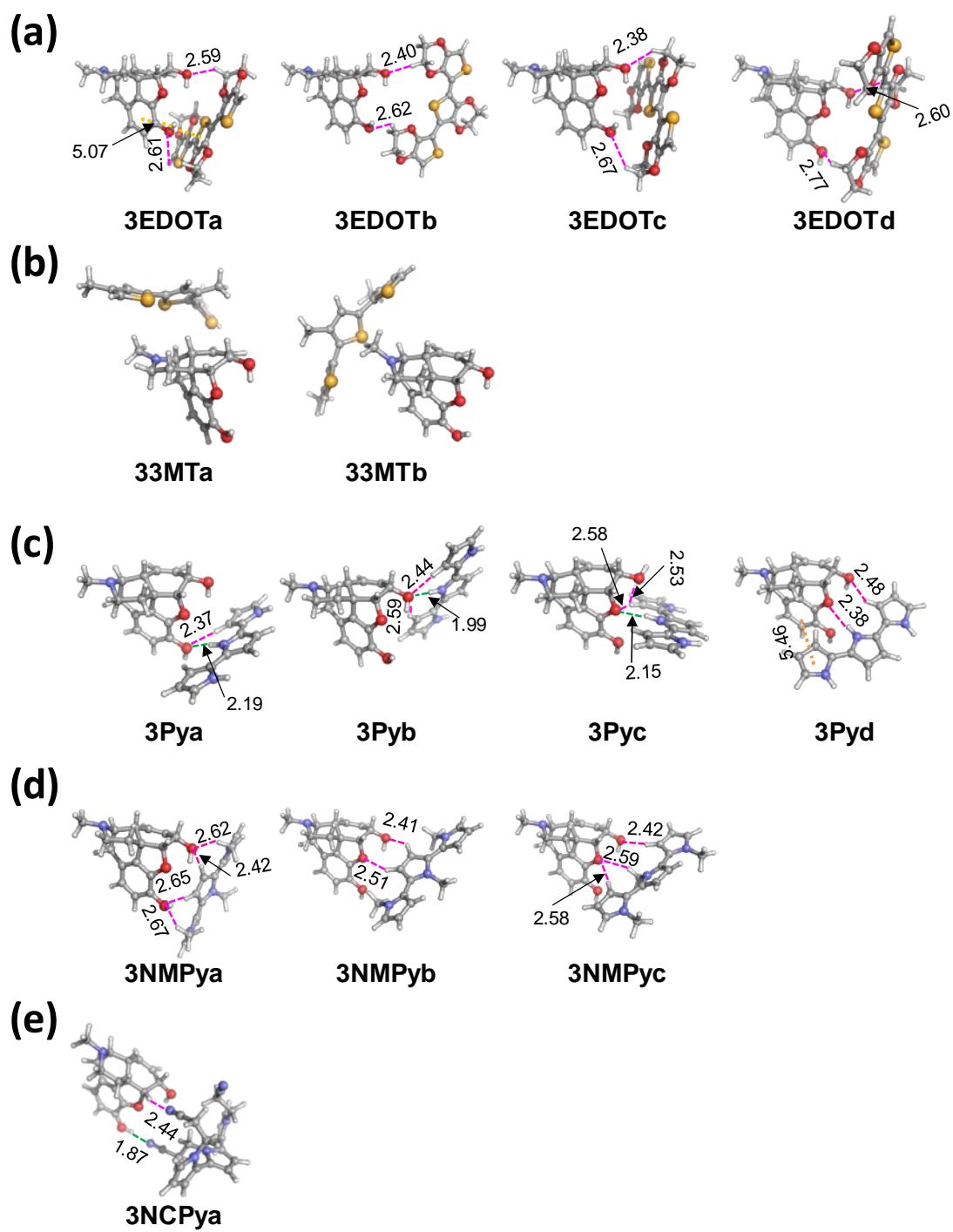


Figure 1

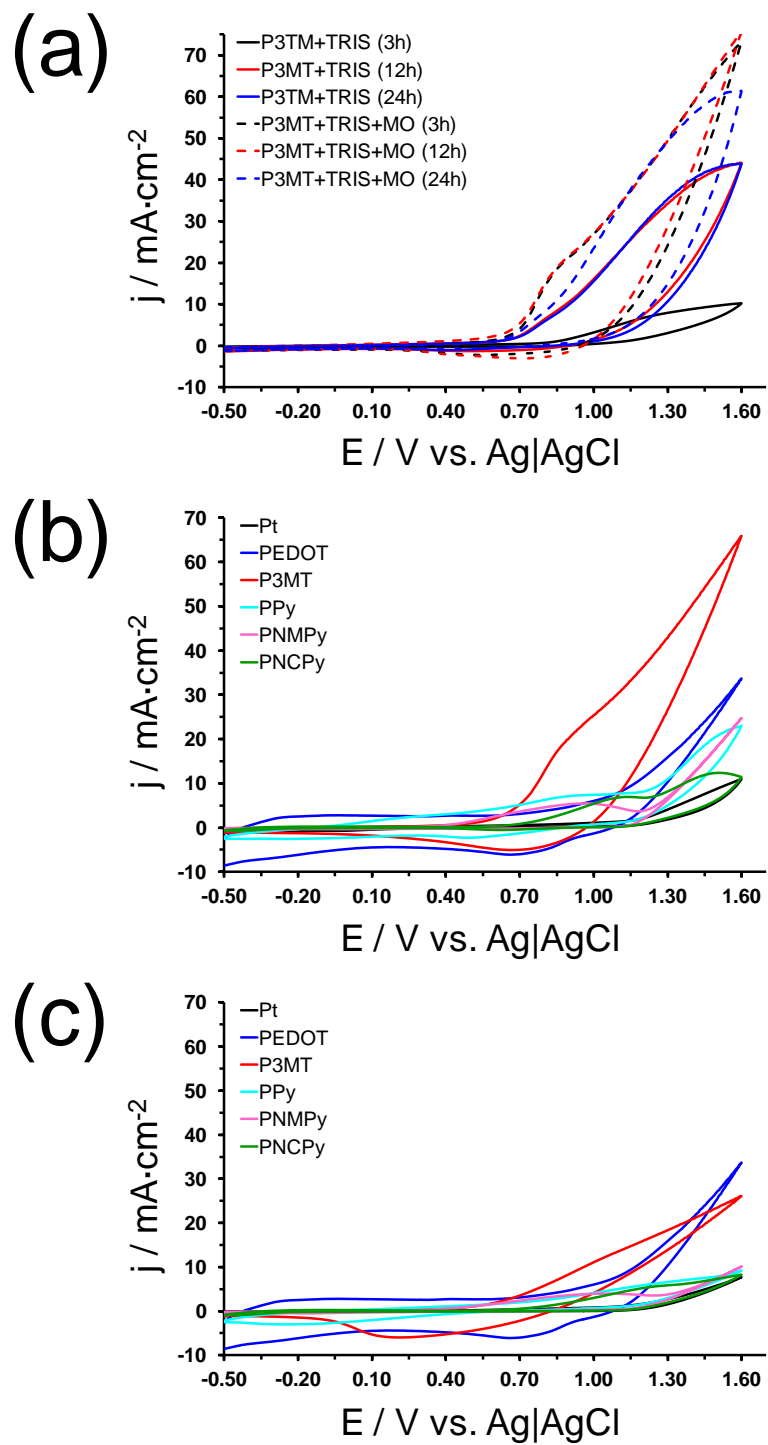


Figure 2

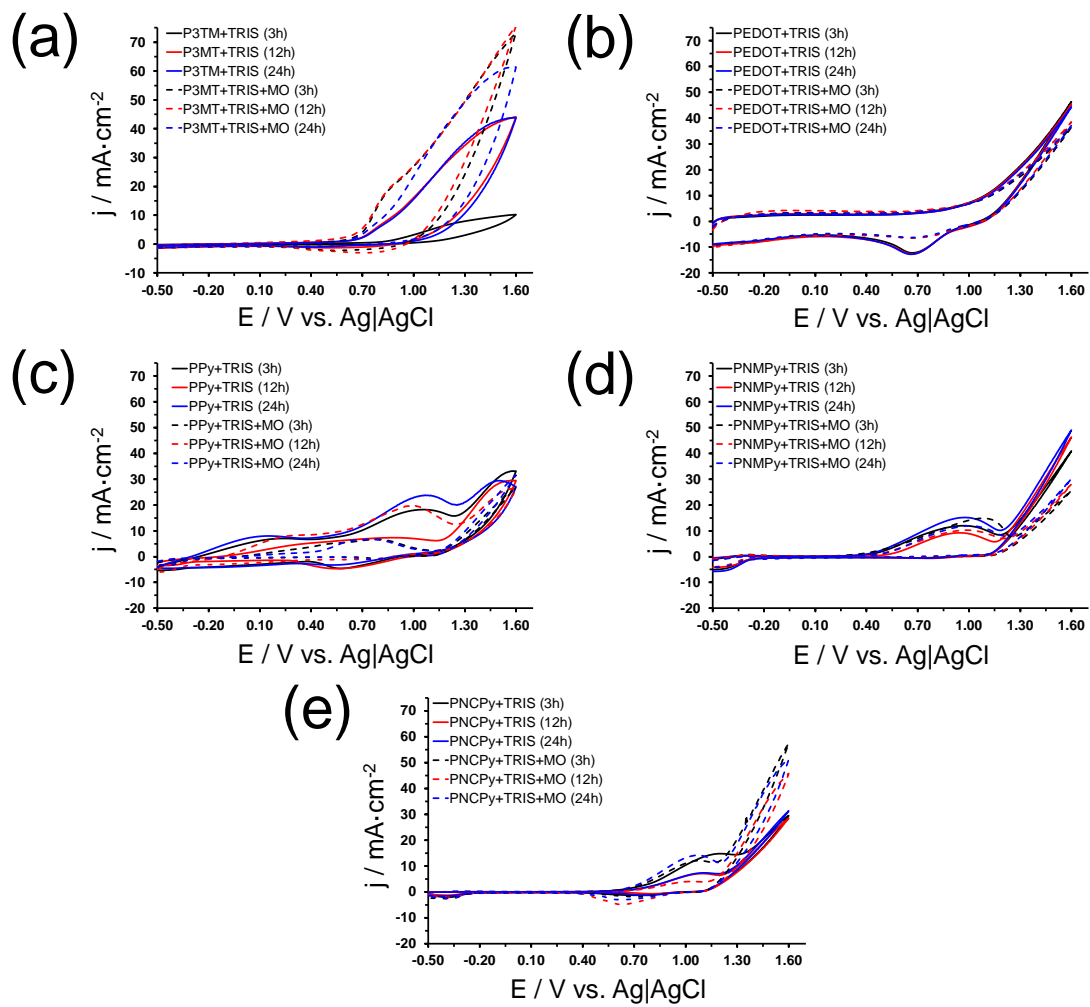


Figure 3

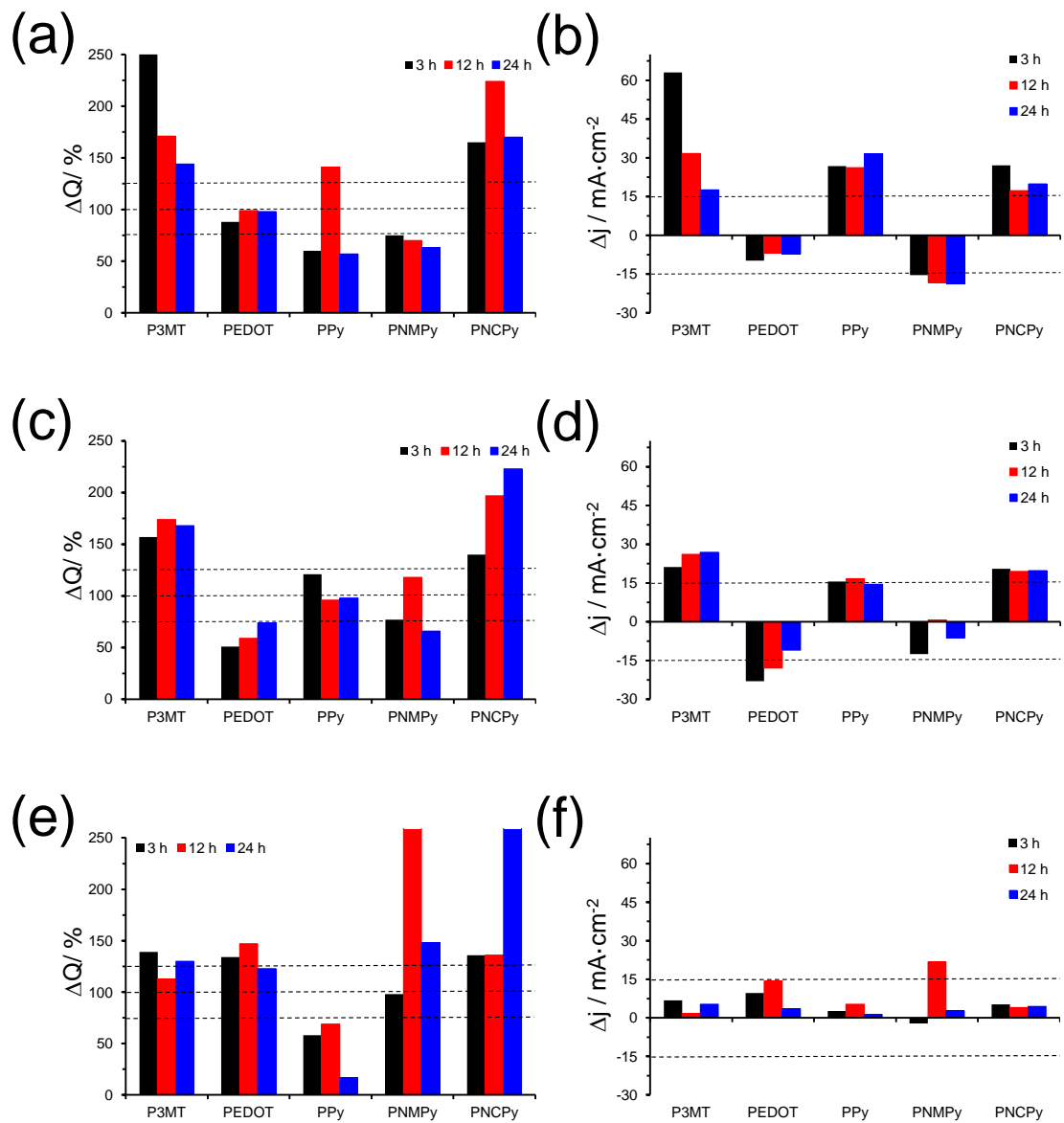


Figure 4

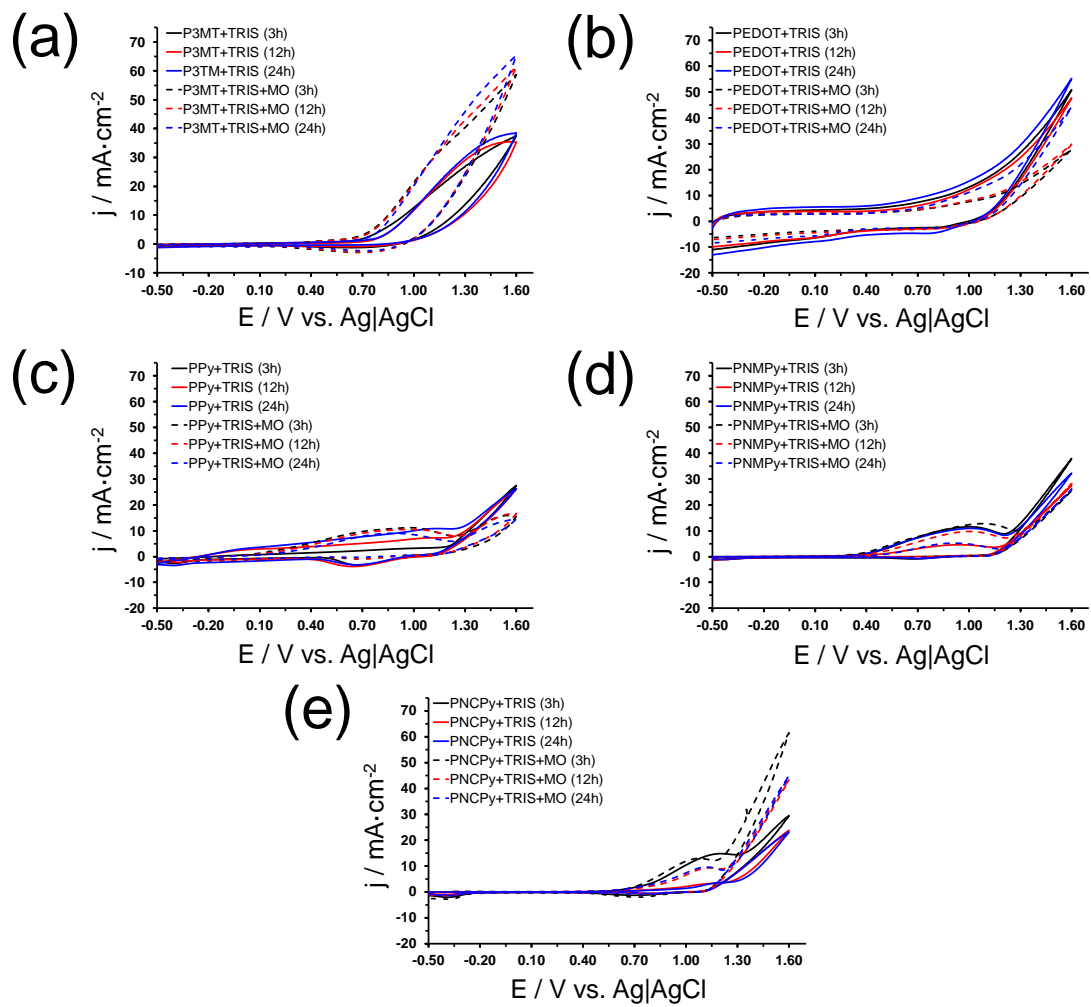


Figure 5

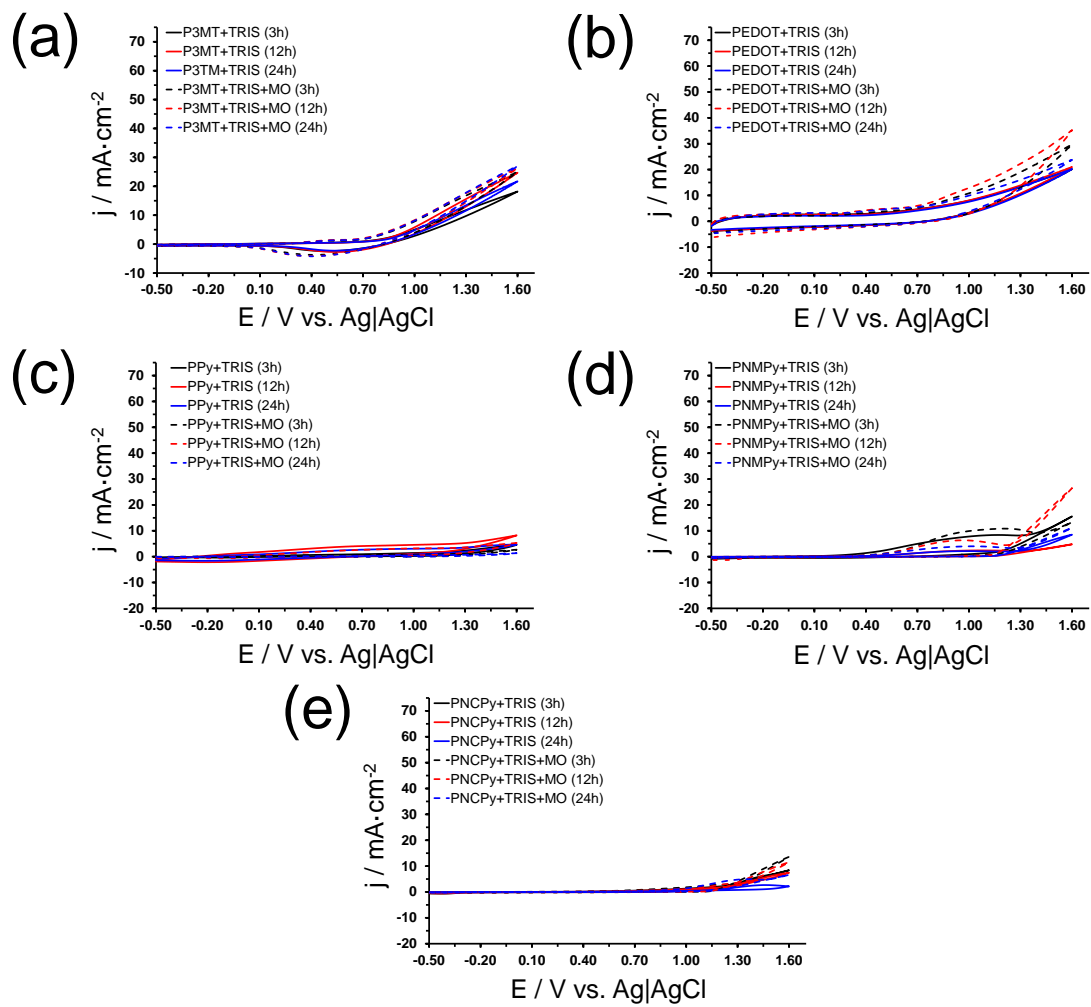


Figure 6

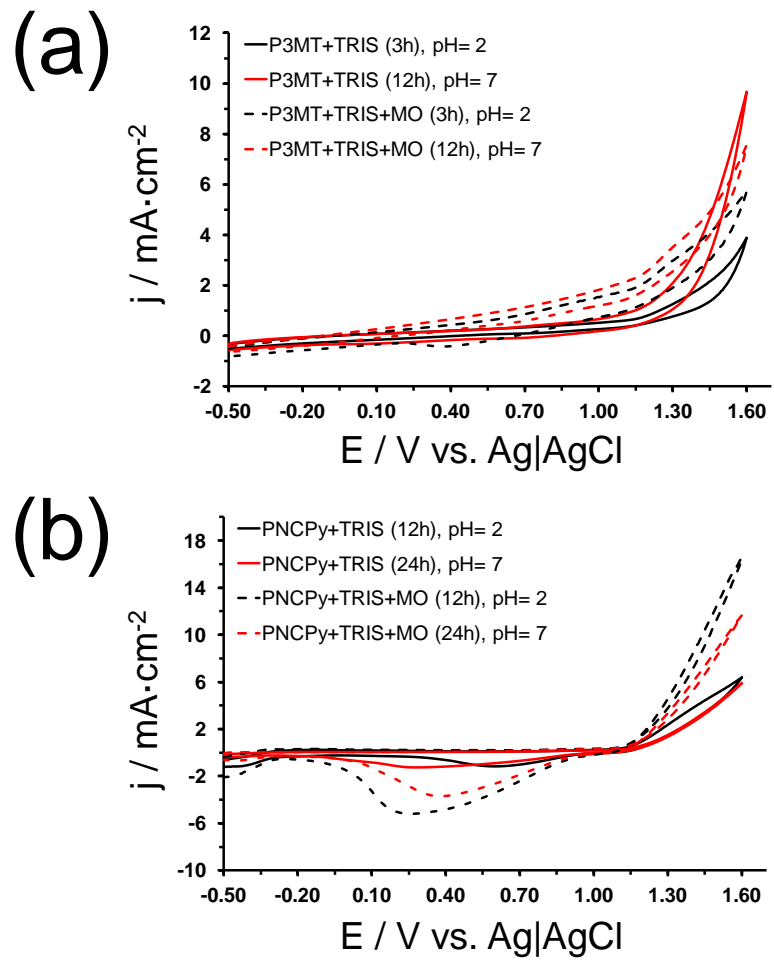


Figure 7